Heating-free, room-temperature operation of a radiofrequency-to-light signal transducer with a membrane oscillator and a built-in metasurface mirror

AUTHOR(S):

Tominaga, Yusuke; Mikami, Atsushi; Iwamura, Akiya; Usami, Koji; Takeda, Kazuyuki

CITATION:

Tominaga, Yusuke ...[et al]. Heating-free, room-temperature operation of a radiofrequency-to-light signal transducer with a membrane oscillator and a built-in metasurface mirror. Applied Physics Express 2022, 15(1): 012003.

ISSUE DATE:

2022-01

URL:

http://hdl.handle.net/2433/276982

Applied Physics Express

The Japan Society of Applied Physics

LETTER • OPEN ACCESS

Heating-free, room-temperature operation of a radiofrequency-to-light signal transducer with a membrane oscillator and a built-in metasurface mirror

To cite this article: Yusuke Tominaga *et al* 2022 *Appl. Phys. Express* **15** 012003

Applied Physics Express **15**, 012003 (2022) **LETTER**
https://doi.org/**10.35848/1882-0786/ac3e15**

Heating-free, room-temperature operation of a radiofrequency-to-light signal transducer with a membrane oscillator and a built-in metasurface mirror

Yusuke Tominaga[1], Atsushi Mikami[1], Akiya Iwamura[2], Koji Usami[2], and Kazuyuki Takeda[1*]

[1]*Division of Chemistry, Graduate School of Science, Kyoto University, 606-8502 Kyoto, Japan*
[2]*Research Center for Advanced Science and Technology (RCAST), The University of Tokyo, Meguro-ku, Tokyo 153-8904, Japan*

[*]E-mail: takezo@kuchem.kyoto-u.ac.jp

Received October 11, 2021; revised November 2, 2021; accepted November 29, 2021; published online December 9, 2021

We present an electro-mechano-optical radiofrequency (rf)-to-light signal transducer robust against laser heating and thus operational at room temperature. A metal-free, low-loss metasurface mirror and an aluminum electrode made separately on a Si_3N_4 membrane oscillator comprise a chain of electro-mechanical and opto-mechanical systems, mediating electrical and optical signals through the (2,2)-mode characteristic oscillation. We demonstrate up-conversion of rf signals at 175.2 MHz by 6 orders of magnitude in frequency to an optical regime with the transfer efficiency of 2.3×10^{-9}, also showing stable operation due to reduced laser heating of the mirror. © 2021 The Author(s). Published on behalf of The Japan Society of Applied Physics by IOP Publishing Ltd

Up-conversion of electrical signals from a radiofrequency (rf) to an optical regime through a chain of electro-mechanical and opto-mechanical systems[1–14] is promising in various circumstances. One direction of research is toward the application of rf-to-light transduction to nuclear magnetic resonance (NMR) and magnetic resonance imaging[15–18] at ambient temperatures using a metal-coated silicon nitride (Si_3N_4) membrane oscillator, by letting the metal layer serve for both an electrode of a capacitor comprising a resonant rf circuit and one of the optical mirrors of an optical cavity. Toward efficient rf-to-light signal transduction, the number of the photons in the optical cavity is desirable to be as large as possible up to the point where the fluctuation of the oscillator due to the radiation pressure of the photons becomes significant.[19–21] However, the optical power is by far limited, not because of the radiation pressure of the photons but of the effect of heating, when the metal layer coated on the membrane serves for the mirror.

Here, we propose an rf-to-light transducer using a low-loss, metal-free mirror and a *separate* metal capacitor electrode implemented on a single Si_3N_4 membrane oscillator. The idea is to exploit a high-order mode of membrane's characteristic oscillation, which has more than one antinodes. By placing the electrode and the mirror such that both contain the antinodes, the separated electrode and mirror can be implemented without sacrificing the strengths of both the electro-mechanical and opto-mechanical couplings. In this work, we make use of the (2,2)-mode characteristic oscillation, employing a vacuum-deposited aluminum electrode and a built-in *metasurface* mirror. The metasurface, also known as a photonic crystal slab, is composed of a horizontal subwavelength-sized structure that reflects light at specific wavelengths.[22–26] In the following, we describe the transducer, evaluate the optical performance and mechanical characteristics, and demonstrate rf-to-light signal transduction. As shown below, the transducer is much less affected by laser heating compared to the previous rf-to-light transducer using the metal mirror on the membrane, allowing for long-term, stable operation at ambient temperatures.

We made metasurface mirrors on a Si-frame supported, 200 nm thick Si_3N_4 membrane with a lateral size of 1 mm × 1 mm by means of electron beam lithography and dry etching, following the procedure reported by Chen et al.[23] First, electron beam resist (ZEP-520A, Zeon) was spin-coated on the membrane, and an array of circles with a radius of 290 nm and a pitch of 830 nm was drawn with an electron beam lithography system (ELS-F125HS, Elionix). Then, the membrane was soaked in development solution (ZED-N50, Zeon) for 250 s and rinsed with isopropanol, before being processed with dry etching with CF_4 plasma. Finally, the electron beam resist remaining on the membrane was removed with O_2 plasma and washed off in dimethylacetamide. A scanning electron microscope (SEM) image showed the periodic array of the holes as designed [Fig. 1(a)]. As shown in Fig. 1(b), we made a diagonal pair of 400 μm × 400 μm square-shaped metasurfaces on the membrane. One of the two mirrors is used to form an optical cavity, while the other served for a spare and testing purposes. In addition, the higher symmetry of the diagonal metasurface mirrors compared to the single metasurface on a quadrant of the membrane is expected to exhibit a cleaner (2,2)-mode of characteristic oscillation.

On the other diagonal part, an aluminum layer with a thickness of 40 nm serving for one of the capacitor electrodes was vacuum deposited. The counter electrode and pillars were made on a printed circuit board [Fig. 1(c)], which was piled on the membrane. The gap between the electrodes determined by the height of the pillar was 1.5 μm. The capacitance was measured to be 3.0 pF.

Figure 2(a) shows a diagram of the transducer. To avoid air damping of the oscillator, the membrane was put inside a vacuum chamber equipped with a window for optical access and a pair of hermetic ports for electrical connection. The membrane capacitor and a solenoid coil outside the chamber formed an LC resonant circuit at 175.2 MHz. To feed rf signals externally, an additional saddle coil was placed and impedance matched at the same frequency. The axes of the two coils were set normal to each other, so as to couple them through mutual inductance only weakly. The measured coupling was −28.7 dB. Using the metasurface mirror and a normal, dielectric, concave cavity mirror with reflectivity of 95% outside the chamber, we assembled an optical cavity with the designed length 47.3 mm of the optical path between

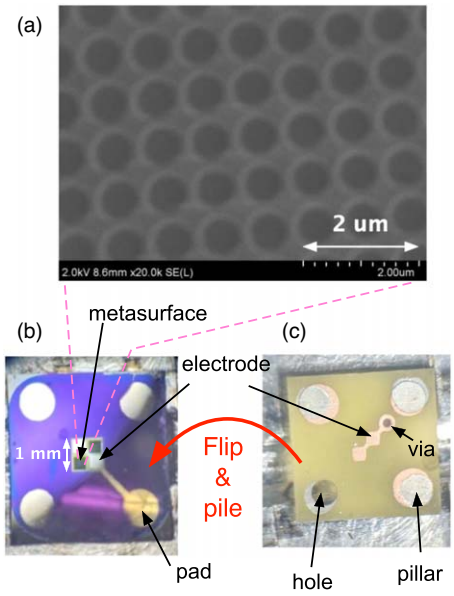

Fig. 1. (Color online) (a) A SEM image of the metasurface. (b) A 1 mm × 1 mm Si_3N_4 membrane, on which a diagonal pair of metasurfaces and a vacuum-deposited Al electrode are made. (c) A printed circuit board serving for the counter electrode of the capacitor.

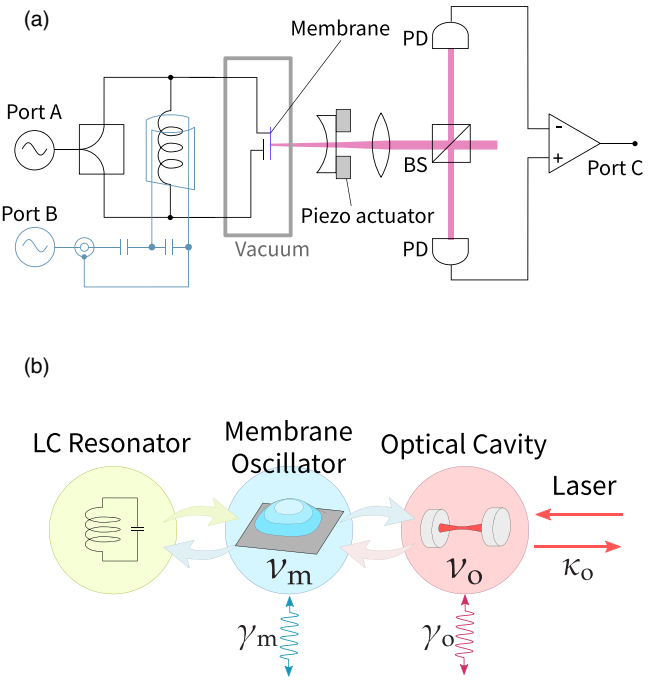

Fig. 2. (Color online) (a) A schematic diagram of the system. BS and PD indicate beamsplitter and photo-detector, respectively. (b) The pathway of signal transduction, where ν_m, and ν_o, are the mechanical and optical frequencies, and κ_o is the external coupling rate of the optical cavity. γ_m and γ_o are membrane and optical-cavity decay rates.

the two mirrors. A piezoelectric actuator served for fine adjustment. A laser beam with a waist radius of 2.03 mm fed into and reflected back from the cavity was guided to a photo-detector. A part of the incident laser beam divided by a beam splitter was sent to another photo-detector, and the difference of the photo-detected signals was monitored on an oscilloscope and a spectrum analyzer. The differential mode acquisition realized shot-noise limited photo-detection. Figure 2(b) describes the pathway of successive signal

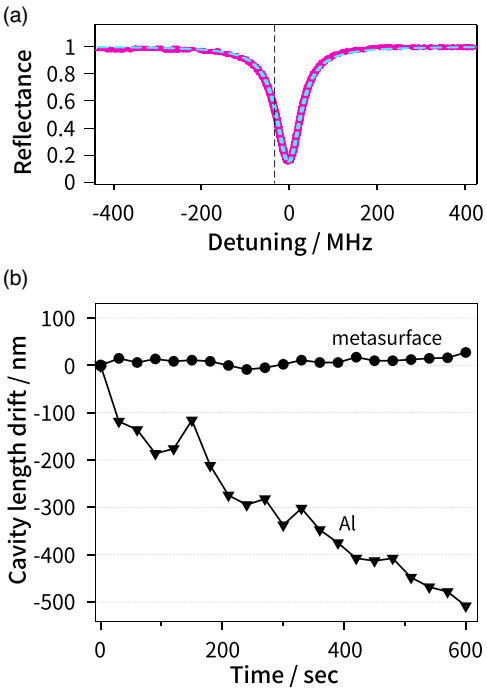

Fig. 3. (Color online) (a) (Solid line) Reflectance of the optical cavity at 1049.16 nm as a function the displacement of the cavity mirror. The horizontal axis is scaled to the detuning in units of frequency. (Broken line) Lorentzian fitting. The vertical broken line indicates the detuning condition used to measure the optical signals in the following measurements. (b) Circles represent change in the optical-cavity length under continuous application of a laser beam with power of 0.35 mW. Triangles show the fluctuation obtained under the same condition except that a vacuum-deposited aluminum mirror is used instead of the built-in metasurface mirror.

transduction from the LC circuit to the membrane oscillator, and finally to the optical cavity.

Figure 3(a) shows measured reflection of a laser beam with a wavelength of 1049.16 nm from the optical cavity as a function of the cavity length. From the finnese of the cavity of ca. 47, the reflectivity of the metasurface was obtained to be 93% at 1049.16 nm. Importantly, most of the residual fraction (7%) of the laser beam just transmitts through the metasurface, and has little contribution to heat dissipation on the membrane.

To evaluate the stability of the transducer against laser irradiation at the membrane, we made for comparion an aluminum mirror on the membrane for the end mirror of the cavity. The measured length of the cavity using the aluminum-coated membrane decreased by up to 500 nm, whereas the metasurface mirror showed little drift for the same laser-beam intensity, as demonstrated in Fig. 3(b).

Let us suppose that an aluminum layer with area of 5×10^{-7} m^2 and thickness of 3.5×10^{-8} m receives a laser beam with power of 19 mW (the power 0.4 mW of the incident beam times the cavity finnese 47), out of which 5% dissipates as heat. Then, from the density 2.697×10^3 kg m^{-3} and the heat capacity 24.34 J K^{-1} mol^{-1} of aluminum, the upper limit of the rate of increase in the temperature is estimated to be as high as 2.2×10^4 K s^{-1}. Even though heat would in reality diffuse to the membrane and then to the silicon frame so that the aluminum would not be heated this much, this crude but simple estimation tells the significance of the effect of heating.

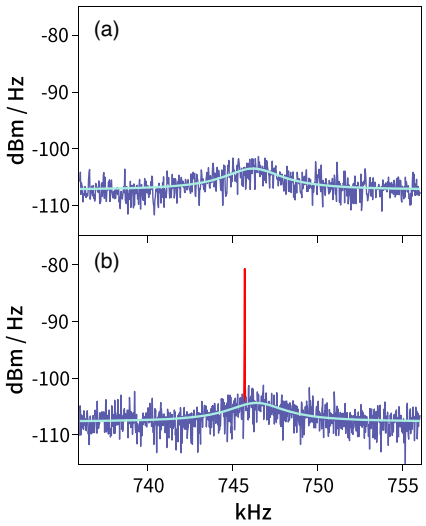

Fig. 4. (Color online) (a) Power spectral density of the optical signal reflected back from the cavity of the transducer, showing the Brownian motion of the (2,2)-mode characteristic oscillation of the membrane. (b) was obtained under application of a tone signal together with a drive signal to the LC circuit. Light-blue lines indicate Lorentzian fitting.

By fixing the detuning of the optical cavity to the condition indicated by the broken line in Fig. 3(a), we monitored the power spectrum of the light reflected back from the cavity, and observed peaks at ca. 452 kHz (not shown) and ca. 746 kHz [Fig. 4(a)] We assigned them to be the Brownian motion of the membrane appearing on the fundamental (1,1)-mode and the (2,2)-mode of characteristic oscillation, respectively. The line was well fitted with a Lorentz function. Its width γ_m was $2\pi \cdot 3500$ Hz, which is rather large compared to that reported in literature, but is suitable for our future applications to NMR requiring the detection bandwidth of the same order.[18] The main cause for the damping is ascribed to the design of the aluminum layer coating across the boundary of the membrane onto the insulated Si frame [Fig. 1(b)].[27] Indeed, we observed much narrower line (not shown) of the power spectrum of the membrane without the aluminum electrode. The frequency $\nu_{j,k}$ of the (j,k)-mode of characteristic oscillation is given by $\nu_{j,k} = \sqrt{(T/4\rho d^2)}\sqrt{j^2 + k^2}$, where T is the tensile stress, ρ is the mass density, and d is the side length of the membrane.[28] With $\rho = 3.2$ g·cm^{-3}, $d = 1$ mm, and the nominal value $T = 1$ GPa, we estimate $\nu_{1,1}$ and $\nu_{2,2}$ for the bare membrane to be 395 kHz and 790 kHz, respectively. The discrepancy from the observed values is ascribed to the diagonal periodic holes and the aluminum coating that affect the local mass density.

To demonstrate rf-to-light signal transduction mediated by the (2,2)-mode characteristic oscillation, we applied to the LC circuit a continuous-wave tone signal at a frequency ν_t of 175.2 MHz through port A indicated in Fig. 2(a) and a drive signal through port B at 175.946 MHz, which corresponds to the sum of the tone frequency and the eigenfrequency 746 kHz of the (2,2)-mode. The tone signal was applied such that the power P_t of the tone signal developed in the LC circuit was -69.7 dBm. Figure 4(b) shows an optically acquired power spectrum of the (2,2)-mode characteristic oscillation with power P_D of the drive signal of 2 dBm, where a sharp peak compared to that of the Brownian motion appeared. When the drive input was turned off for comparison, the peak disappeared, so that it indeed originates from the successfully transduced tone signal.

As increasing the power P_D of the drive signal, the power of the transduced tone signal increased as well, showing linear dependence, as indicated by the red circles in Fig. 5. Here, the vertical axis was scaled to the number $\dot{N}_o$ of the *optical* photons per unit time, which is given by Ref. 15

$$\dot{N}_o = \frac{\kappa_o}{\kappa_o + \gamma_o} C_{om} C_{em} \frac{P_t}{h\nu_t}, \tag{1}$$

where κ_o and γ_o are the external coupling rate and the internal decay rate of the optical cavity [see Fig. 2(b)], and h is the Planck constant. C_{om} and C_{em} are optomechanical and electromechanical cooperativities,[1] which measure the efficiency of signal transfer between the two oscillators. Conversely, the arrival rate $\dot{N}_m$ of photons transduced from the Brownian noise of the membrane oscillator, also plotted in Fig. 5, is expressed as Ref. 15

$$\dot{N}_m = 2\frac{\kappa_o}{\kappa_o + \gamma_o} C_{om} \gamma_m \frac{kT}{h\nu_m}, \tag{2}$$

where $\nu_m = 746$ kHz is the mode frequency, γ_m is the mechanical damping rate, k is the Boltzmann constant, and T is temperature. From measured values $\kappa_o = 2\pi \times 20.8$ MHz, $\gamma_o = 2\pi \times 46.6$ MHz, and $\gamma_m = 2\pi \times 3.5$ kHz, we obtained the optomechanical cooperativity $C_{om} \approx 2.2 \times 10^{-6} \times (P_L/\text{mW})$ for a given power P_L of the laser beam. From the drive-power dependence of the photon-arrival rate $\dot{N}_o$, we estimate C_{em} to be $\approx 7.5 \times 10^{-5} \times (P_D/\text{mW})$. We find that the current value of C_{em} for a given drive power P_D is comparable to that in our previous work.[18] Thus, the current (2,2)-mode-mediated transduction was reasonably efficient.

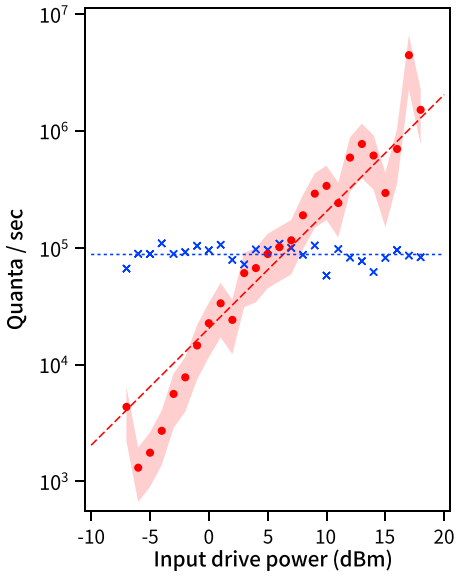

Fig. 5. (Color online) The rate of arrival of the transduced photons carrying the tone signals (circles) and noise (diagonal crosses) as a function of the drive power. Lines represent linear fitting. The error in the number of the quanta per unit time, indicated by the shaded area, arises from the fluctuation of the length of the optical cavity, which was estimated from the data shown in Fig. 3(b) to be ca. 8 nm. The noise photon arrival rate was estimated from the integral of the Lorentzian line shown in Fig. 4 that corresponds to the Brownian noise.

The average number of the optical photons transduced from a single rf photon measures the overall signal transfer efficiency. From Eq. (1), the transfer efficiency is given by $[\kappa_o/(\kappa_o+\gamma_o)]C_{om}C_{em}$. With the maximum attainable laser power, 0.44 mW, in our current experimental setup, the transfer efficiency is $\approx 2.3\times10^{-9}$ with a moderate drive power of 20 dBm. Now that the transducer was found to be robust against laser heating, the transfer efficiency would further be improved by employing the laser beam with higher power.

In this work, we demonstrated signal transduction using the (2,2)-mode. Extension to other modes of characteristic oscillation is straightforward. Our ultimate goal is to acquire rf signals, in the form of optically up-converted ones, with higher sensitivity than that of traditional electrical detection at room temperature. Since the Johnson noise intrinsic to the LC circuit is faithfully transduced in both cases, noise added through the process of acquisition matters. In electrical detection, an amplifier used in the first stage has the main contribution to added noise. Conversely, it is the Brownian noise of the membrane that counts, when the contribution of the optical shot noise is much smaller. It is desirable to increase the efficiency of signal transduction from the electrical to the mechanical system to such an extent that the transduced Johnson noise accompanying the target rf signal overwhelms the mechanical Brownian noise of the membrane oscillator. In our previous proof-of-principle demonstrations of transducing rf NMR signals to light, the efficiency of signal up-conversion was comparable to that in this work. However, fluctuation of the optical cavity over time of the order of no more than several minutes was so serious that long-term operation of NMR measurement was not possible. Now that stable operation of the transducer has been realized, NMR analysis of materials of chemical/biological interests, which can take hours or even days, has become realistic. Our research in the future directs toward the operation of the transducer at ambient temperature in superconducting magnets conventionally used for NMR systems dedicated for chemical analysis. To further improve the transduction efficiency, it would be desirable to increase the electro-mechanical coupling strength by reducing the gap of the membrane capacitor.[15)]

Acknowledgments We are grateful to P.-F. Cohadon and S. Deléglise for inspiring us and fruitful discussions. We thank S. Iwamoto, K. Kusuyama and Y. Nakamura for valuable inputs on metasurface mirrors. This work has been supported by JST CREST (Grant No. JPMJCR1873), JST ERATO (Grant No. JPMJER1601) and Grants-in-Aid for JSPS Fellows (Grant No. 20J14033).

ORCID iDs Kazuyuki Takeda https://orcid.org/0000-0002-6743-0932

1) T. Bagci et al., "Optical detection of radio waves through a nanomechanical transducer," Nature **507**, 81 (2014).
2) R. W. Andrews, R. W. Peterson, T. P. Purdy, K. Cicak, R. W. Simmonds, C. A. Regal, and K. W. Lehnert, "Bidirectional and efficient conversion between microwave and optical light," Nat. Phys. **10**, 321 (2014).
3) L. Midolo, A. Schliesser, and A. Fiore, "Nano-opto-electro-mechanical systems," Nat. Nanotechnol. **13**, 11 (2018).
4) A. P. Higginbotham, P. S. Burns, M. D. Urmey, R. W. Peterson, N. S. Kampel, B. M. Brubaker, G. Smith, K. W. Lehnert, and C. A. Regal, "Harnessing electro-optic correlations in an efficient mechanical converter," Nat. Phys. **14**, 1038 (2018).
5) M. Forsch, R. Stockill, A. Wallucks, I. Marinković, C. Gärtner, R. A. Norte, F. van Otten, A. Fiore, K. Srinivasan, and S. Gröblacher, "Microwave-to-optics conversion using a mechanical oscillator in its quantum ground state," Nat. Phys. **16**, 69 (2020).
6) Y. Chu and S. Gröblacher, "A perspective on hybrid quantum opto- And electromechanical systems," Appl. Phys. Lett. **117**, 150503 (2020).
7) G. Arnold, M. Wulf, S. Barzanjeh, E. S. Redchenko, A. Rueda, W. J. Hease, F. Hassani, and J. M. Fink, "Converting microwave and telecom photons with a silicon photonic nanomechanical interface," Nat. Commun. **11**, 4460 (2020).
8) J. M. Fink, M. Kalaee, R. Norte, A. Pitanti, and O. Painter, "Efficient microwave frequency conversion mediated by a photonics compatible silicon nitride nanobeam oscillator," Quantum Sci. Technol. **5**, 034011 (2020).
9) X. Han, W. Fu, C.-L. Zou, L. Jiang, and H. X. Tang, "Microwave-optical quantum frequency conversion," Optica **8**, 1050 (2021).
10) J. Bochmann, A. Vainsencher, D. D. Awschalom, and A. N. Cleland, "Nanomechanical coupling between microwave and optical photons," Nat. Phys. **9**, 712 (2013).
11) A. Vainsencher, K. J. Satzinger, G. A. Peairs, and A. N. Cleland, "Bi-directional conversion between microwave and optical frequencies in a piezoelectric optomechanical device," Appl. Phys. Lett. **109**, 033107 (2016).
12) K. C. Balram, M. I. Davanço, J. D. Song, and K. Srinivasan, "Coherent coupling between radiofrequency, optical and acoustic waves in piezo-optomechanical circuits," Nat. Photonics. **10**, 346 (2016).
13) X. Han et al., "Cavity piezo-mechanics for superconducting-nanophotonic quantum interface," Nat. Commun. **11**, 3237 (2020).
14) W. Jiang, C. J. Sarabalis, Y. D. Dahmani, R. N. Patel, F. M. Mayor, T. P. McKenna, R. Van Laer, and A. H. Safavi-Naeini, "Efficient bidirectional piezo-optomechanical transduction between microwave and optical frequency," Nat. Commun. **11**, 1166 (2020).
15) K. Takeda, K. Nagasaka, A. Noguchi, R. Yamazaki, Y. Nakamura, E. Iwase, J. M. Taylor, and K. Usami, "Electro-mechano-optical detection of nuclear magnetic resonance," Optica **5**, 152 (2018).
16) A. Simonsen, S. A. Saarinen, J. D. Sanchez, J. H. Ardenkjr-Larsen, A. Schliesser, and E. S. Polzik, "Sensitive optomechanical transduction of electric and magnetic signals to the optical domain," Opt. Express. **27**, 18561 (2019).
17) A. Simonsen, J. D. Sánchez-Heredia, S. A. Saarinen, J. H. Ardenkjr-Larsen, A. Schliesser, and E. S. Polzik, "Magnetic resonance imaging with optical preamplification and detection," Sci. Rep. **9**, 18173 (2019).
18) Y. Tominaga, K. Nagasaka, K. Usami, and K. Takeda, "Studies on NMR-signal up-conversion from radio-frequency to optical regimes using a lightweight nanomembrane transducer," J. Magn. Reson. **298**, 6 (2019).
19) O. Arcizet, P.-F. Cohadon, T. Briant, M. Pinard, and A. Heidmann, "Radiation-pressrure cooling and optomechanical instability of amicro-mirror," Nature **444**, 71 (2006).
20) J. D. Teufel, T. Donner, M. A. Castellanos-Beltran, J. W. Harlow, and K. W. Lehnert, "Nanomechanical motion measured with precision beyond the standard quantum limit," Nat. Nanotechnol. **4**, 820 (2009).
21) T. P. Purdy, R. W. Peterson, and C. A. Regal, "Observation of radiation pressureshot noise on a macroscopic object," Science **339**, 801 (2013).
22) S. Fan and J. D. Joannopoulos, "Analysis of guided resonances in photonic crystal slabs," Phys. Rev. B **65**, 235112 (2002).
23) X. Chen et al., "High-finesse Fabry–Perot cavities with bidimensional Si_3N_4 photonic-crystal slabs," Light Sci. Appl. **6**, e16190 (2017).
24) P. Qiao, W. Yang, and C. J. Chang-Hasnain, "Recent advances in high-contrast metastructures, metasurfaces, and photonic crystals," Adv. Opt. Photonics **10**, 180 (2018).
25) J. Martínez-Llinàs, C. Henry, D. Andrén, R. Verre, M. Käll, P. Tassin, and A. Gaussian, "Reflective metasurface for advanced wavefront manipulation," Opt. Express. **27**, 21069 (2019).
26) J. Hu, S. Bandyopadhyay, Y. H. Liu, and L. Y. Shao, "A review on metasurface: from principle to smart metadevices," Front. Phys. **8**, 1 (2021).
27) P.-L. Yu, T. P. Purdy, and C. A. Regal, "Control of material damping in high-Q membrane microresonators," Phys. Rev. Lett. **108**, 083603 (2012).
28) D. Wilson, C. Regal, S. Papp, and H. Kimble, "Cavity optomechanics with stoichiometric SiN Films," Phys. Rev. Lett. **103**, 207204 (2009).